ESEEM Study of the Plastoquinone Anion Radical ($Q_A^{\bullet -}$) in ^{14}N- and ^{15}N-Labeled Photosystem II Treated with CN[†]

Yiannis Deligiannakis,*[,‡] Alain Boussac, and A. William Rutherford

Section de Bioénergétique, URA CNRS 1290, Département de Biologie Cellulaire et Moléculaire, CEA Saclay, 91191 Gif-sur-Yvette, France

Received July 13, 1995; Revised Manuscript Received October 2, 1995[⊗]

ABSTRACT: The nonheme iron of the photosystem II reaction center was converted to its low-spin state (S = 0) by treatment with CN^-. This allowed the study of the plastoquinone, Q_A^- anion radical by electron spin-echo envelope modulation (ESEEM) spectroscopy. A comparative analysis of the ESEEM data of Q_A^- in ^{14}N- and ^{15}N-labeled PSII demonstrates the existence of a protein nitrogen nucleus coupled to the Q_A^-. The ^{14}N coupling is characterized by a quadrupolar coupling constant $e^2qQ/4h = 0.82$ MHz, an asymmetry parameter $\eta = 0.45$, and hyperfine coupling constant $A \sim 2.1$ MHz. The ^{15}N hyperfine coupling is characterized by $T = 0.41$ MHz and $\alpha_{iso} \sim 3.3$ MHz. The possible origins of the nitrogen hyperfine coupling are discussed in terms of the amino acids thought to be close to the Q_A^- in PSII. Based on a comparison of the ^{14}N ESEEM with ^{14}N-NQR and ^{14}N-ESEEM data from the literature, the most likely candidate is the amide nitrogen of the peptide backbone of Ala261 of the polypeptide D2, although the indole nitrogen of Trp254 and the imino nitrogen of His215 of D2 also remain candidates.

In the photosystem II (PSII)[1] reaction center a plastoquinone-9 (Q_A) and a pheophytin-α molecule mediate the photoinduced electron transfer from the primary donor, P_{680}, to a plastoquinone pool [for a review see Hansson and Wydrzynski (1990)]. These molecules are magnetically coupled with a nonheme Fe^{2+} (S = 2) atom (Klimov et al., 1980; Nugent et al., 1981; Rutherford & Zimmermann, 1984) which in its native environment is in the high-spin state and does not play a direct redox role in the electron transfer (Petrouleas & Diner, 1987). A similar situation occurs in the reaction center of the purple bacteria and has been analyzed in detail by Butler et al. (1984). According to this analysis, because of the magnetic coupling with the iron, the EPR spectrum of the Q_A^- is severely broadened and extends over several hundred Gauss. Furthermore, in the bacterial reaction center the spin lattice relaxation of the state Q_A^- Fe^{2+} is fast even at cryogenic temperatures (Calvo et al., 1982). In PSII the only resolvable part of the EPR spectrum of the ferrosemiquinone complex, Q_A^- Fe^{2+} (S = 2), is characterized by features around g = 1.90 and 1.84, depending on the pH (Rutherford & Zimmerman, 1984) and the specific molecules bound in the vicinity of the nonheme iron (Vermaas & Rutherford, 1984; Koulougliotis et al., 1993; Deligiannakis et al., 1994).

For a thorough understanding of the details of the electron transfer reactions, a knowledge of both the spatial arrangement and the electronic structure of the primary reactants in the reaction center is essential. In this context the study of the hyperfine interactions of the semiquinone radical with the surrounding nuclei can give valuable information concerning the electronic structure and the function of the reaction center. Electron nuclear double resonance (ENDOR) and electron spin-echo envelope modulation (ESEEM) are the appropriate techniques for performing hyperfine spectroscopy. For the detection of weak hyperfine couplings in complex immobilized radicals, ESEEM spectroscopy is the method of choice (Dikanov & Tsvetkov, 1992 and references therein). The very fast spin lattice relaxation of Q_A^- Fe^{2+} (S = 2) and the excessive broadening of its EPR signal have prevented the application of these techniques using the native PSII reaction center. An alternative is to remove the iron. In the bacterial reaction center, a protocol for the reversible extraction of the iron and its replacement by other metals, like Zn, has been developed by Debus et al. (1986). Although Klimov et al. (1980) were able to remove the iron from PSII, this was only partially reversible, and the replacement of the iron by other metals was not reported. More recently, some attempts to remove and/or to replace the iron by other metals have been reported (Akabori et al., 1992; MacMillan et al., 1990, 1995), although the intactness of the reaction center and the completeness of the metal replacement have not been evaluated. In a ^1H-ENDOR study of plastoquinone radicals *in vitro* and in Fe^{2+}-depleted PSII reaction centers (MacMillan et al., 1990, 1995) the hyperfine couplings of the semiquinone radical with methyl- and matrix-protons were reported.

Recently, Sanakis et al. (1994) have shown that treatment of the PSII with CN at alkaline pH (8.0−8.5) converts the nonheme iron to the low-spin diamagnetic state (S = 0). This offers an alternative way for studying the semiquinone radical when decoupled from the iron. In this paper, we report the

[†] This work was supported by the European Union H.C.M. network "MASIMO", Contract ERBCHRXCT920072.

* Corresponding author.

[‡] On leave from the Institute of Materials Science, NCSR "Democritos", 15310 Aghia Paraskevi Attikis, Greece.

[⊗] Abstract published in *Advance ACS Abstracts,* December 1, 1995.

[1] Abbreviations: PSII, photosystem II; Q_A, the primary electron acceptor of the iron−quinone complex; Tyr Y_D, tyrosine radical responsible for the EPR signal II_{slow}; HEPES, 4-(2-hydroxyethyl)-1-piperezineethanesulfonic acid; MES, 2-(*N*-morpholino)ethanesulfonic acid; Tris, tris(hydroxymethyl)aminomethane; ESEEM, electron spin-echo envelope modulation; c.w. EPR, continuous-wave electron paramagnetic resonance; NQI, nuclear quadrupole interaction.

0006-2960/95/0434-16030$09.00/0

ESEEM study of the semiquinone anion radical in PSII reaction center treated with CN^- in order to convert the nonheme iron to the low spin state. The comparative analysis of the ESEEM data of the Q_A^- radical in ^{14}N- and ^{15}N-labeled PSII reaction centers demonstrates the existence of a super-hyperfine interaction between the semiquinone radical and a protein nitrogen nucleus.

MATERIALS AND METHODS

PSII membranes were isolated from market spinach as described previously (Berthold et al., 1891) with the modifications described in Boussac & Rutherford (1988). ^{15}N-labeled membranes were prepared from spinach grown in a medium supplemented with ^{15}N-labeled minerals [98% $K^{15}NO_3$, $(^{15}NH_4)_2SO_4$, and $Ca(^{15}NO_3)$, Eurisotop, Saclay, France] as described in Zimmermann et al. (1993). Tris treatment was performed by incubating these PSII membranes (0.5 mg of chlorophyll/mL) in 0.8M Tris-HCl (pH 8.3), 5 mM NaEDTA for 30 min at 0 °C under room light. The Tris-treated membranes were pelleted and washed once in a buffer containing 60 mM HEPES (pH 8.0), 10 mM NaCl, 5 mM $MgCl_2$ and resuspended in the same buffer at 5 mg chl/mL final concentration. The nonheme iron was converted to its low-spin state by incubating the Tris-treated PSII membranes with 350 mM $KC^{14}N$ at pH 8.0 for 3 h at 5 °C, according to Sanakis et al. (1994). A similar procedure was followed by using $KC^{15}N$ (99.4% ^{15}N, ISOTEC inc., OH, USA). The Q_A^- radical was induced by subsequent incubation of the membranes under reducing conditions (E_h = −250 ± 20 mV) for 30 min/5 °C, in the dark. The redox potential was adjusted by sodium dithionite under anaerobic conditions and was measured in the sample with a platinum electrode, with a calomel reference electrode (Russell pH, Auchtermuchty, UK) connected to a Tacussel pH/millivolt meter (Tacussel, Villeurbanne, France). Measured redox potentials were normalized to the standard hydrogen electrode, calibrating the electrode using saturated quinhydrone (potential = 286 mV, at pH 6.5). Quantitation of the formation of the Q_A^- radical was done by comparison with the double integral of the EPR spectrum of the stable tyrosine radical in untreated PSII according to Buser et al. (1992).

Continuous-wave (c.w.) EPR spectra were recorded at liquid helium temperatures with a Bruker ER 200D X-band spectrometer equipped with an Oxford Instruments cryostat. The microwave frequency and the magnetic field were measured with a microwave frequency counter HP 5350B and a Bruker ER035M NMR gaussmeter, respectively. Pulsed EPR was performed with a Bruker ESP 380 spectrometer with a dielectric resonator, described in Zimmermann et al. (1993); typical instrument deadtime was 100 ns. The comparison of the modulation patterns recorded at various temperatures between 4 and 80 K showed that the acquisition temperature has no effect on the modulation frequencies; the data presented here were recorded at 45 K. The two-pulse ESEEM was measured by detecting the amplitude of the echo resulting from a $\pi/2-\tau-\pi$ microwave sequence as a function of the interpulse time τ which was incremented by 8-ns steps, the $\pi/2$ pulses, ~300 W, were of 8-ns duration. Dead-time reconstruction was performed according to Mims (1984). In the three-pulse ($\pi/2-\tau-\pi/2-T-\pi/2$) ESEEM data, the amplitude of the simulated echo as a function of $\tau + T$ was measured at a frequency near 9.6 GHz at a magnetic field corresponding to the maximum intensity of the field swept spectrum. The minimum interpulse T was 16 ns and was incremented in steps of 8 ns; the duration of the $\pi/2$ pulse was 16 ns. To remove the unwanted echoes in a three-pulse experiment, the phase cycling procedure described in Fauth et al. (1986) was applied. Before Fourier transform, the time domain echo decay was factored out by subtraction on a sixth-order polynomial (two-pulse data) or a linear (three-pulse data) function. The field swept spectra were obtained by recording the amplitude of the echo as a function of the magnetic field after a two-pulse sequence ($\pi/2-144ns-\pi$); the duration of the $\pi/2$ and π pulse was 32 and 64 ns, respectively.

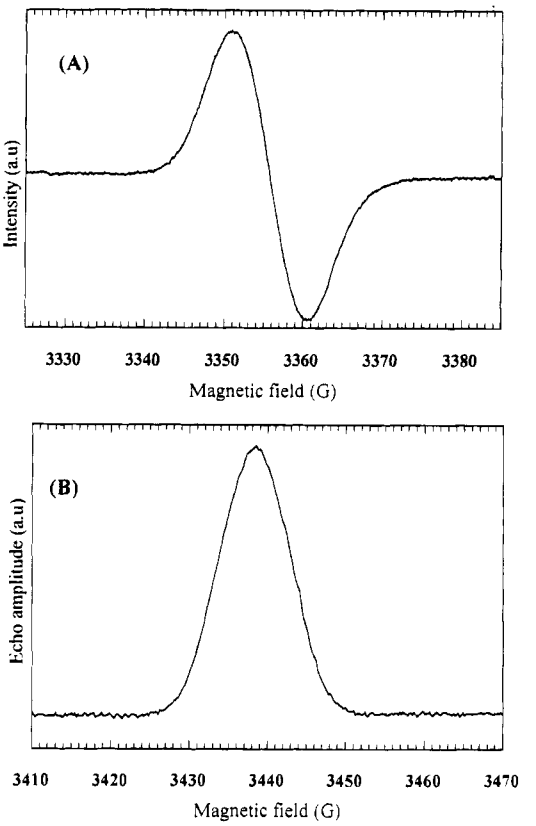

FIGURE 1: (A) X-band c.w. EPR spectrum of Q_A^- in dithionite-reduced (E_h = −250 mV), Tris-washed ^{14}N-PSII membranes (5 mg chl/mL) treated with 340 mM KCN. Experimental conditions: sample temperature, 15 K; microwave frequency, 9.415 GHz; microwave power, 50 μW; modulation amplitude, 2 G; modulation frequency, 12.5 kHz. (B) Amplitude of the electron spin echo of $Q_A^{\bullet -}$ resulting from a two-pulse sequence, as a function of the magnetic field. The same sample as in (A) was used. Experimental conditions: sample temperature, 45K; τ, 144 ns; time interval between successive pulse sets, 3 ms; microwave frequency, 9.64 GHz.

RESULTS

The continuous wave (c.w.) X-band EPR spectrum of reduced PSII membranes treated with CN^- is depicted in Figure 1A. Under these conditions the stable $TyrD^+$ radical is reduced and the PSII reaction center is in the state Q_A^- Fe^2 (S = 0) (Sanakis et al., 1994); thus the only detected radical is Q_A^-. The EPR spectrum is characteristic of the plastoquinone anion radical decoupled from the iron—i.e., a structureless derivative with g = 2.0045 ± 0.0002 and ΔH = 9.5 ±0.3 G (Klimov et al., 1980; Sanakis et al., 1994). In Figure 1B the echo-detected field-swept spectrum of this sample is displayed. The spectrum is a 9.0 ± 0.5 G wide

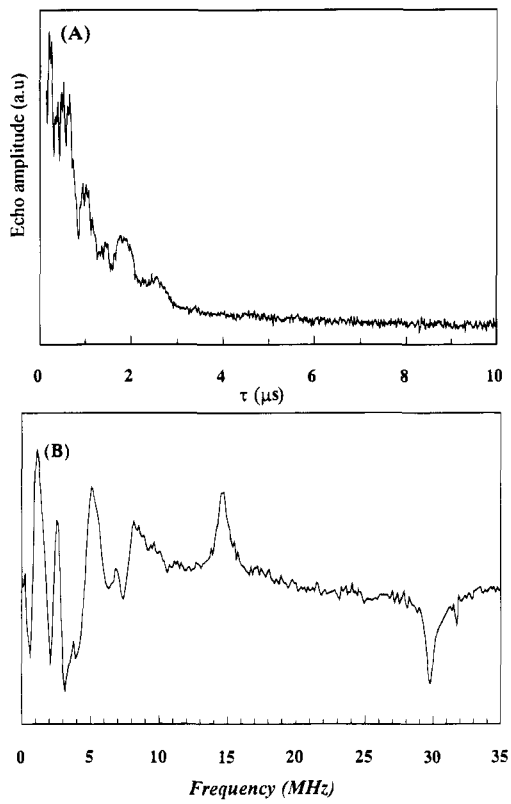

FIGURE 2: Primary echo ESEEM signal (A) and cosine Fourier transform (B) of Q_A^- in ^{14}N-PSII treated with CN. Experimental conditions: microwave frequency, 9.64 GHz; magnetic field strength, 3438 G; sample temperature, 45 K; initial τ value, 120 ns; 1024 data points collected at 16-ns intervals.

absorption line with maximum intensity at $g = 2.0045 \pm 0.0003$. No other signals are detected in the 2−4 kG magnetic field range.

ESEEM in ^{14}N-PSII. In Figure 2A the decay of the time-domain two-pulse ESE trace is displayed. This has been recorded at a static magnetic field H = 3438 G corresponding to the maximum intensity of the echo-detected field-swept spectrum; the ^{14}N Larmor frequency in the this case is ν_I = 1.06 MHz. In the frequency-domain (Figure 2B) several components are revealed. The frequency-domain spectrum of the primary echo decay, contains not only the nuclear transition frequencies but probably also their sum and difference (Mims, 1972a,b) making the assignment of the lines cumbersome. Furthermore, when there is anisotropic hyperfine coupling it may happen that only the combination lines are resolved (Reijerse & Dikanov, 1991; Dikanov & Tsvetkov, 1992). These limitations can be circumvented by performing stimulated-echo experiments. In this case, the echo decay is determined only by the spin-lattice relaxation, and, at least when one nucleus is considered, it is modulated by the fundamental nuclear transition frequencies without their sums or differences (Mims, 1972a,b).

Figure 3A displays the stimulated-echo decay. In order to avoid missing modulation frequencies due to suppression effects (Mims & Peisach, 1981), the echo decay was recorded at several τ values. The echo decays slowly as is expected from the long T_1 of the Q_A^- radical at this temperature (45 K) (Koulougliotis et al., 1994). The corresponding frequency-domain spectra are depicted in Figure 3B; the trace in Figure 3C is a "suppression free" spectrum which is the sum of the Fourier transform of the stimulated echo ESEEM recorded at 24 τ values (from 120 ns to 504 ns in steps of 16 ns). Four frequency components are resolved: three narrow lines with peaks at 0.73, 2.08, and 2.81 MHz and a broad line with a maximum at ~ 5.25 MHz. A weaker line at 1.4−1.5 MHz can also be resolved especially at τ values where the stronger lines are suppressed, and at low τ-values a broad shoulder at 4.6−4.8 MHz is seen which is absent at higher τ values.

The fact that the sum of the 0.73 MHz and 2.08 MHz frequencies equals the 2.81 MHz frequency is a characteristic indication that these peaks arise from ^{14}N (I = 1) nuclear modulation [Mims & Peisach, 1978; Dikanov et al., 1982; see also Romanelli et al. (1988) for a review]. In this case, the three narrow low-frequency components arise from that ^{14}N superhyperfine spin manifold, where the nuclear-Zeeman and electron-nuclear hyperfine interaction approximately cancel each other, so that the level splittings are primarily determined by the ^{14}N nuclear quadrupole interaction (NQI) (Flanagan & Singel, 1987). In the case of exact cancellation, these almost pure quadrupolar lines have no anisotropy broadening, and they are sharp, while a moderate deviation from the exact cancellation drastically reduces the intensities of the observed peaks whereas their positions remain almost constant. In the case of exact cancellation, the ESEEM spectrum contains three sharp low-frequency lines, with maxima at frequencies given by the relations

$$\nu_+ = K(3 + \eta), \nu_- = K(3 - \eta), \nu_0 = 2K\eta \qquad (1)$$

where $K = e^2Qq_{zz}/4h$ is the quadrupole coupling constant, Q is the scalar quadrupole moment, $\eta = (q_{xx} - q_{yy})/q_{zz}$ is the asymmetry parameter of the electric field gradient $\{g_{ii}, i = x, y, z\}$ at the nucleus and x, y, z are the principal axes of the quadrupole coupling tensor. Computer simulations of ^{14}N ESEEM under conditions of exact cancellation showed that the positions of the lines are determined by the values of K and η, while their relative intensities are sensitive to the relative orientation of the NQI principal axes system with respect to the hyperfine coupling tensor and the τ value used for the measurement (Flanagan & Singel, 1987; Cornelius et al., 1990). In the present case, the detected lines at 0.73, 2.08, and 2.81 MHz according to eq 1 yield $K = 0.82$ MHz and $\eta = 0.45$.

The superhyperfine manifold, where the nuclear-Zeeman and the hyperfine interactions are additive, gives rise to much broader resonances (Dikanov et al., 1982; Flanagan & Singel, 1987) and the only resolvable component is a double quantum transition line, $\Delta m_I = 2$, occurring at higher frequencies. The double-quantum line has maximum intensity at a frequency which is approximated by

$$\nu_{dq} \approx 2[(\nu_I + A/2)^2 + K^2(3 + \eta^2)]^{1/2} \qquad (2)$$

where A is a secular component of the hyperfine coupling tensor determined mainly from its isotropic part; a modest anisotropy of the hyperfine interaction affects mainly the lineshape but not the frequency of the double quantum line (Flanagan & Singel, 1987; Reijerse & Keijzers, 1987). In the present case, the double-quantum line has maximum intensity at 5.25 MHz; thus for the calculated values of K and η, eq 2 results in $A \sim 2.1$ MHz. For this value of A and $\nu_I = 1.06$ MHz, the exact cancellation condition is fulfilled

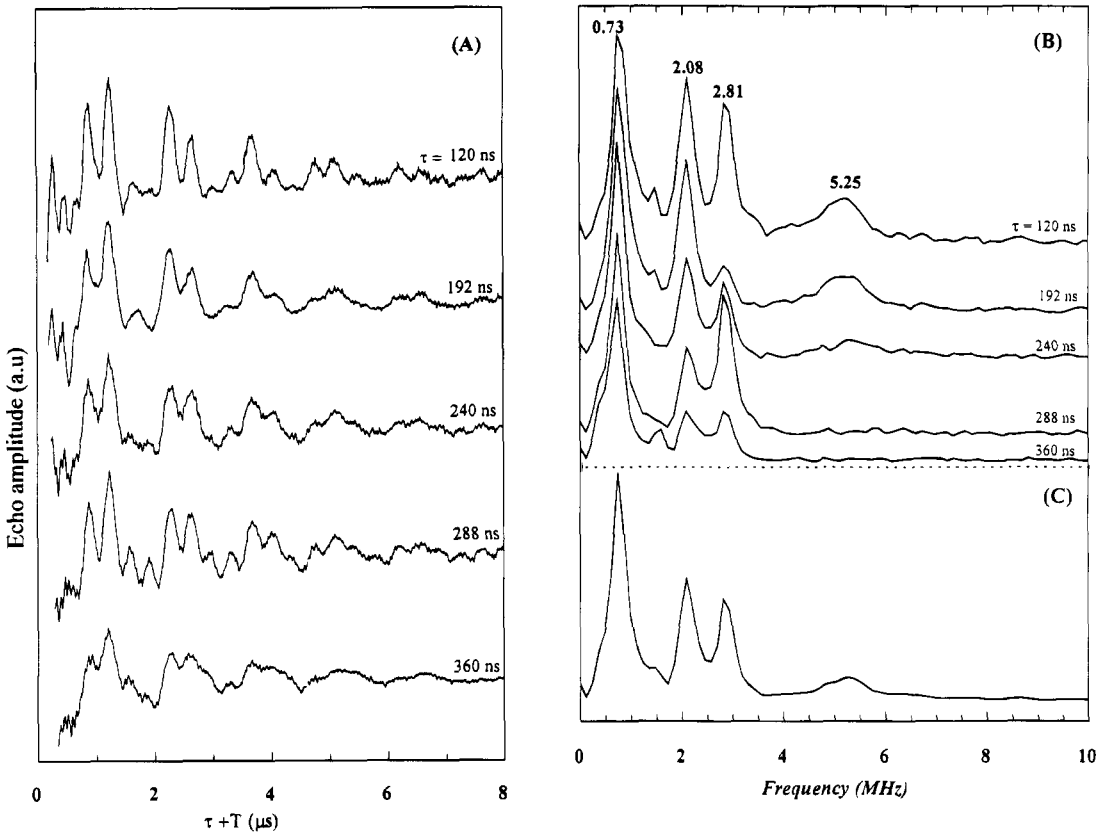

FIGURE 3: (A) Stimulated echo ESEEM signal of Q_A^- in ^{14}N-PSII treated with CN recorded at the indicated τ values (period between first and second microwave pulses). (B) Power calculation of the Fourier transform. (C) Sum of the Fourier transform of stimulated echo ESEEM recorded at 24 τ values, from 120 to 504 ns in increments of 16 ns. Experimental conditions: microwave frequency, 9.64 GHz; magnetic field strength, 3438 G; sample temperature, 45 K; time interval between successive pulse sets, 3 ms; 200 events were averaged for each time point. For each τ value the initial T value (period between second and third microwave pulses) was 16 ns, and 1024 data points were collected at 8-ns intervals; a four-step phase cycle was employed.

($A/2 = \nu_I$).[2] It is of interest to note that in the present case the value of K is comparable with $A/2$ which is the "intermediate K region" according to Flanagan and Singel (1987). In this case under the condition of exact cancellation and $\eta > 0$, the double-quantum line is split; this splitting is manifested as a shoulder superimposed on the double quantum line on its low-frequency side (Flanagan & Singel, 1987); moreover, a weak anisotropic hyperfine coupling or a misalignment of the principal axis systems of the hyperfine interaction and NQI tensors would result in a splitting and broadening of the double quantum line (Reijerse & Keijzers, 1987). In accord with this analysis, the feature at 4.6−4.8 MHz which is seen in Figure 3C could be part of the double quantum line rather than a separate component.

Although the above theoretical analysis is strongly indicative for the interpretation of the data, in order to assign rigorously the nitrogen transitions we have carried out ESEEM measurements in ^{15}N-labeled PSII.

ESEEM in ^{15}N-PSII. The primary-echo decay of Q_A^- in ^{15}N-PSII treated with CN^-, is displayed in Figure 4A. The corresponding frequency-domain spectrum, is depicted in Figure 4B. The field-swept spectrum, presented in the inset of Figure 4A, is similar to that recorded in ^{14}N-PSII.

From Figures 4B and 2B is is easily seen that, although the matrix proton lines at ~15 and ~30 MHz are present in both spectra, the low-frequency part of Figure 2B is different from that of Figure 4B. The differences between the ESEEM in the ^{14}N- and ^{15}N-labeled PSII can be analyzed in more detail by comparing the stimulated-echo data which are presented in Figure 5A. These spectra were recorded at several τ values under the same experimental conditions that were used for the acquisition of the ESEEM data in ^{14}N-PSII. A deep modulation of the echo decay with a period ~3 μs is the dominating feature of the spectra. In addition, two shallower modulation harmonics with periods of ~1.4 μs and ~0.3 μs can be resolved at certain τ values. The corresponding frequencies can be analyzed by referring to the frequency-domain spectra that are presented in Figure 5B. A "suppression free" spectrum is displayed in the inset of Figure 5B; it is the sum of the Fourier transform of the ESEEM recorded at 24 τ values (from 120 ns to 888 ns in steps of 32 ns). In the low-frequency part of Figure 5B an intense line with maximum at 0.31 MHz, and a weaker one at 2.92 MHz are the main components of the spectra. These correspond to the ~3 μs and ~0.3 μs modulation periods, respectively. By comparison of Figures 5B and 3B, it is immediately seen that the four main low-frequency lines of Figure 3B are absent in Figure 5B. This allows an unequivocal assignment of these lines to nitrogen modulations (summarized in Table 1).

[2] A reviewer pointed out that by using the ^{14}N coupling parameters given here ($A \sim 2.1$ MHz, $K = 0.82$ MHz, $\eta = 0.45$) simulations of the ESEEM spectra show a shift from 4.9 to 5.4 MHz for the maximum intensity of the double quantum line, when the principal axes of the hyperfine and nuclear quadrupole interaction tensors are taken from being collinear to perpendicular. Such a shift would result in a ±0.3 MHz deviation from the coupling we report ($A \sim 2.1$ MHz) and does not significantly change the main conclusion we make about the cancellation condition.

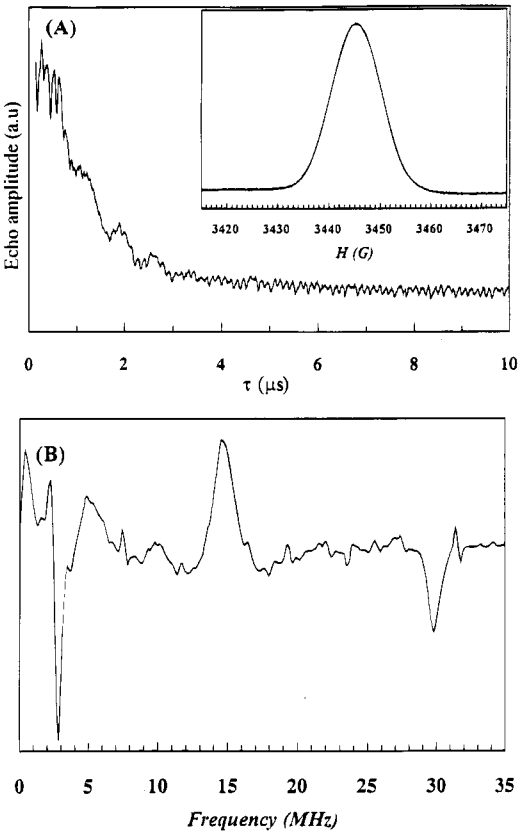

FIGURE 4: Primary echo ESEEM signal (A) and cosine Fourier transform (B) of Q_A^- in ^{15}N-labeled PSII treated with CN. Experimental conditions: microwave frequency, 9.66 GHz; magnetic field strength, 3443 G; sample temperature, 45 K; time interval between successive pulse sets, 3 ms; initial τ value, 120 ns; 1024 data points were collected at 16-ns intervals. *Inset* in panel A: field-swept ESE detected spectrum of the Q_A^- in ^{15}N-labeled PSII.

In the ESEEM spectrum of the ^{15}N-labeled PSII, Figure 5B, the weak lines at frequencies 0.73, 2.08, and 2.81 MHz, which can be resolved at certain τ values, coincide with those detected in the ESEEM of Q_A^- in ^{14}N-PSII, Figure 3B. This raises the possibility that some fraction of the detected ^{14}N modulation may originate from the cyanide nitrogen since in all these experiments, the PSII membranes were treated with $C^{14}N$. This molecule binds in the vicinity of the nonheme iron in competition with bicarbonate (Koulougliotis et al., 1993; Sanakis et al., 1994). In order to clarify this point, we have carried out ESEEM measurements of Q_A^- in ^{14}N-PSII membranes treated with $C^{15}N$. No differences were observed between the ESEEM of Q_A^- in PSII treated with $C^{14}N$ or $C^{15}N$ (data not shown). Thus, the fractional ^{14}N modulation detected in the ^{15}N-labeled PSII is attributed to ^{14}N nuclei due to incomplete isotopic substitution; this fraction is estimated to be approximately 10−15% (this level of isotopic substitution is to be expected for hydroponically grown plants if one considers the ^{14}N contamination coming from other salts in the media, the vermiculite, and seed).

The line at ~1.5 MHz is present in the ESEEM of Q_A^- in ^{14}N and ^{15}N-labeled PSII as well as in the sample treated with $C^{15}N$; this indicates that it does not originate from a nitrogen nucleus. The most probable nuclei that could be responsible for this modulation are the protons. In an attempt to examine a possible influence of the pH on the ESEEM patterns and on the hydrogen bonding, we have repeated the ESEEM measurements in a ^{14}N-PSII sample treated (at pH 8, 30 mM HEPES) with CN, followed by addition of 200 mM MES (pH 6.0) and incubation for 20 min. The two-pulse and three-pulse data showed no differences in comparison with the spectra presented in Figures 2 and 3 (data not shown).

Theoretical Analysis. In the ESEEM of an S = 1/2, I = 1/2 system, the fundamental hyperfine frequencies for the two electron spin manifolds are given by

$$\nu_\alpha = [(A/2 - \nu_I)^2 + (B/2)^2]^{1/2} \quad (3a)$$

and

$$\nu_\beta = [(A/2 + \nu_I)^2 + (B/2)^2]^{1/2} \quad (3b)$$

where, for an axial nuclear hyperfine coupling in the point-dipole approximation the hyperfine interaction tensor has principal values ($\alpha_{iso} - T$, $\alpha_{iso} - T$, $\alpha_{iso} + 2T$) and

$$A = \alpha_{iso} + T(3\cos^2\theta - 1) \quad (4a)$$

$$B = 3T\cos\theta\sin\theta \quad (4b)$$

$$T = g_n g_e \beta_n \beta_e / hr^3 \quad (4c)$$

In the above relations ν_I is the nuclear Larmor frequency; α_{iso}, the isotropic hyperfine coupling; θ, the angle describing the direction of the laboratory magnetic field with respect to the principal axis of the hyperfine tensor; g_n and g_e are the nuclear and electron g-values; β_n and β_e are the corresponding nuclear and Bohr magneton; and r is the distance of the nucleus from the effective position of the electron (Mims & Peisach, 1978).

In orientationally disordered systems, the lineshapes for the basic ESEEM frequencies ν_α and ν_β are determined by the angular dependence of the line positions, according to eq 3a,b, the modulation depth factor, which is usually written in the form $k = (\nu_I B/\nu_\alpha\nu_\beta)^2$, and the statistical weight factor $^1/_2\sin\theta\, d\theta$. The angular dependence of the modulation depth factor is mainly determined by the B factor; at the canonical directions B is zero and attains its maximum value at intermediate angles, i.e., at $\theta = 45°$ where $B_{max} = 3T/2$. From eq 3a it is seen that in the "matching region", i.e., when $A/2 \sim \nu_I$, the frequency ν_α is determined approximately by the B term. This case has been analyzed by detailed simulations in the frequency domain by several authors (de Groot et al., 1986; Lin et al., 1986; Reijerse & Keijzers, 1987). In a detailed analysis Lai et al. (1988) have shown that in this case an intense line at a position $\nu_\alpha \sim |B_{max}|/2 = 3|T|/4$ is expected in the ESEEM spectrum. In addition, if $\nu_I \sim A/2$ the ν_β transition would result in a line at $\sim 2\nu_I$, which is broader and weaker than the ν_α line. More specifically, in the matching region we have $\nu_I \sim (2\alpha_{iso}+T)/4$ and the frequency position of the ν_β line is $\alpha_{iso}-T < \nu_\beta < \alpha_{iso}+2T$ (Lai et al., 1988). It is important to note that a modest rhombicity of the hyperfine coupling would influence the width but not the center frequency of the intense low-frequency line at ν_α [Lai et al., 1988; see also Gerfen and Singel (1994)]. Thus the determination of $|T|$ from this ESEEM frequency is not affected by the rhombicity of the hyperfine interaction.

In the present case, scaling the calculated ^{14}N hyperfine coupling by the factor $g_n(^{15}N)/g_n(^{14}N) \sim 1.4$ we estimate a value of ~2.9 MHz for the hyperfine coupling of the ^{15}N

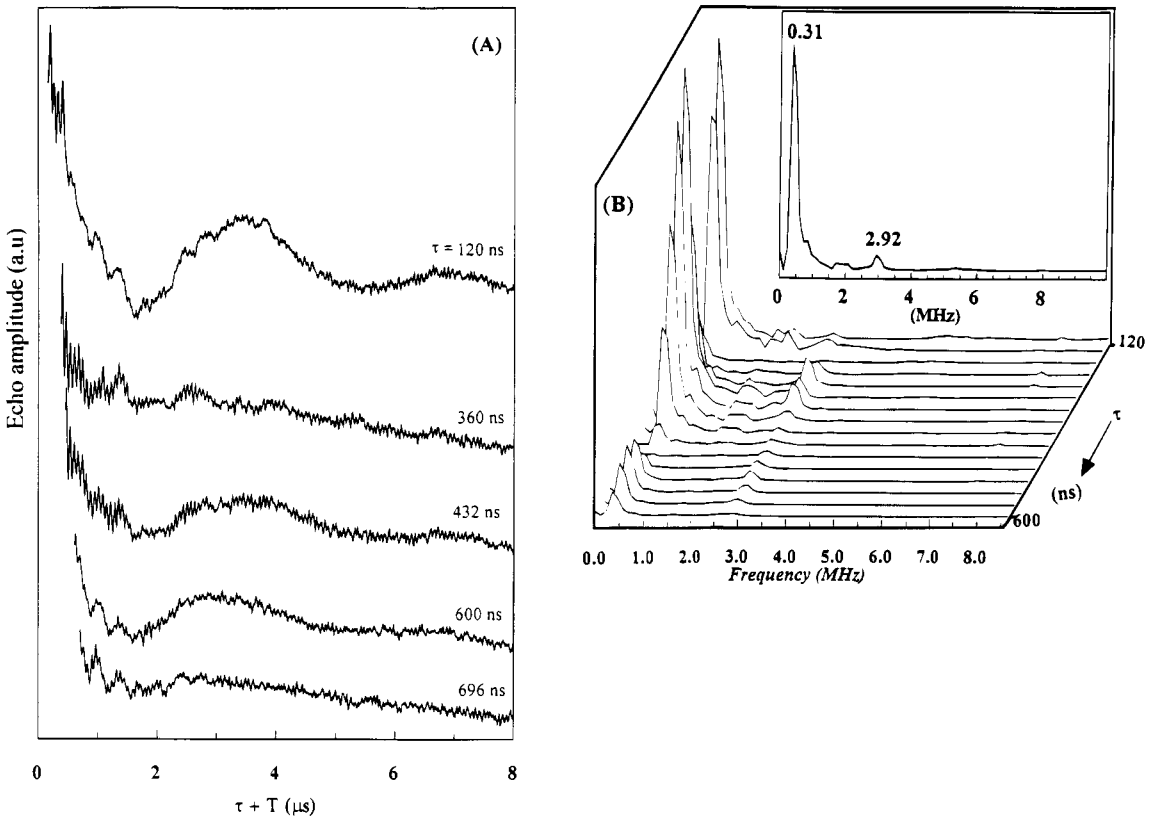

FIGURE 5: (A) Stimulated echo ESEEM signal of Q_A^- in ^{15}N-labeled PSII treated with CN recorded at the indicated τ values. (B) Power calculation of the Fourier transform. The depicted series of ESEEM spectra were recorded at a series of time intervals (τ) between the first and the second microwave pulses. The increment in τ is 32 ns. The amplitude of the observed peak at 0.31 MHz is modulated as a function of τ at the frequency of its partner, ~2.9 MHz. Inset in panel B: Sum of the Fourier transform of stimulated echo ESEEM at 24 τ values from 120 to 888 ns. Experimental conditions: microwave frequency, 9.66 GHz; magnetic field strength, 3443 G; other conditions as in Figure 3.

Table 1: Stimulated-Echo Modulation Frequencies,[a] Nuclear Quadrupole, and Hyperfine Interaction Constants of the Q_A^- Radical in ^{14}N- and ^{15}N-Labeled Photosystem II

^{14}N-PSII[b]				^{15}N-PSII[b]					
ν (MHz)	A (MHz)	K (MHz)	η	ν (MHz)	α_{iso} (MHz)	T (MHz)	K^c (MHz)	η^c	reference
				0.31	3.3	0.41			
0.73									^{14}N-ESEEM
2.08	2.1	0.82	0.45	2.92			0.81	0.45	peptide N[d]
2.81									
5.25									^{14}N-NQR
							0.80−0.84	0.45−0.51	di/tripeptide[e,f]
							0.81−0.83	0.13−0.21	Imino N His[e,f]
							0.31−0.34	0.91−0.97	Amino N His
							0.79	0.18	Indole Trp[f]

[a] Error ± 0.05 MHz. [b] Values in the 7 columns shown represent ESEEM data of $Q_A^{\bullet-}$ in PSII treated with CN. [c] Values of ^{14}N-nuclear quadrupole interaction parameters (K, η) derived from ESEEM or NQR studies. [d] Cammack et al., 1988; Coremans et al., 1995; [e] Ashby et al., 1980; [f] Edmonds 1977; Hund and Macay, 1976.

nucleus, which implies that the condition $A/2 \sim \nu_I$ is valid (at 3443 G the Larmor frequency ν_I of the ^{15}N nucleus is 1.48 MHz). The observed weak line at 2.92 MHz, which is $\sim 2\nu_I$, and the intense low-frequency line at 0.31 MHz are assigned to the frequencies ν_α and ν_β. This assignment is strongly supported if we examine the dependence of the intensities of these two lines on the τ-value as it is seen in Figure 5B. The variation of the intensity of the line at ν_α is characterized by a period corresponding to ~ 2.9 MHz, which is approximately equal to the ν_β; this is due to the suppression effect (Mims, 1972a) and indicates that these two lines correspond to the two fundamental nuclear transitions coupled to the same electron spin. The frequency of the partner of the line at ν_β (i.e., ν_a) is sufficiently small that it is almost suppressed at most of the τ-values [see also Gerfen and Singel (1994)]. According to this analysis we have $3|T|/4 \sim 0.31$ MHz which yields $|T| \sim 0.41$ MHz.

Primary-Echo ESEEM. In the primary-echo ESEEM of orientationally disordered systems, the frequency position of the peak maximum of the combination lines is given by the relation (Reijerse & Dikanov, 1991)

$$(\nu_\alpha \pm \nu_\beta)_{max} = 2\nu_I\,(1 + (3T/4)^2/\{\nu_I^2 - [(T+2\alpha_{iso})/4]^2\})^{1/2} \quad (5a)$$

From this relation if the value of $|T|$ is known, it is possible to estimate the isotropic hyperfine coupling constant from

the frequency of the combination line. The negative phased line at ~2.8 MHz, in Figure 4B, is assigned to a combination line of the two fundamental ^{15}N transitions ν_α, ν_β. From eq. (5a) the two possible values for the isotropic hyperfine coupling of the ^{15}N nucleus are $|\alpha_{iso}|$ ~3.3 or 3.7 MHz; for $|T| = 0.41$ MHz and $\nu_\beta = 2.92$ MHz, the value of 3.3 MHz satisfies the condition $\alpha_{iso}-T < \nu_\beta < \alpha_{iso}+2$ for opposite signs of T and α_{iso}.

When $\alpha_{iso} \ll \nu_I$ the expression (5a) can be approximated by the formula

$$(\nu_\alpha+\nu_\beta)_{max} \approx 2\nu_I+(3T/4)^2/\nu_I \qquad (5b)$$

In Figures 2B and 4B, the line at ~14.7 MHz, corresponds to the Larmor frequency of the free ^1H nucleus, ν_H. In the primary-echo data, a line at 29.8 MHz ~ $2\nu_H$ appears antiphase to the fundamental proton line and is assigned to the sum combination harmonic ($\nu_{\alpha+\beta}$) of very weakly coupled protons (Mims, 1972a,b). Considering that for these protons the isotropic hyperfine interaction is negligible, for $\Delta = |(\nu_\alpha+\nu_\beta)_{max} - 2\nu_I| \sim 0.4$ MHz according to the relation 5b, a value of $|T| \sim 4$ MHz is estimated; however, since this Δ value is close to the frequency resolution of the two-pulse experiment, this estimation should be considered as a upper limit.

DISCUSSION

The characteristic changes observed in the ESEEM of the Q_A^- radical upon isotopic substitution of ^{14}N by ^{15}N unambiguously show that the low-frequency modulations originate from a nitrogen nucleus coupled to the Q_A^-. From existing structural information on PSII it seems clear that the nitrogen originates from the protein environment of Q_A^-. Based on the structural homology of the acceptor sides of the bacterial reaction center and PSII, several amino acid residues have been suggested as forming part of the binding pocket of Q_A in PSII (Trebst, 1986; Michel & Deisenhofer, 1988; Komiya et al., 1988). In *R. viridis* (Michel et al., 1986) and in *R. sphaeroides*, (Ermler et al., 1994) the two oxygens of the Q_A ring are hydrogen-bonded to the peptide nitrogen of Ala M258 and to the amino-nitrogen of the imidazole of His M217. Tryptophan M252 in *R. sphaeroides* (Allen et al., 1988; Ermler et al., 1994) and M250 in *R. viridis* (Michel et al., 1986) is located between the bacteriopheophytin $Bpheo_A$ and the quinone Q_A, and it is postulated that it plays a role in the electron transfer process. Its indole ring is in van der Waals contact with Q_A, although its exact positioning relative to the π-system of the quinone is different in the two species [Allen et al., 1988; Ermler et al., 1994; see also Plato et al. (1989)]. All these residues appear to be conserved in PSII: the Trp 254, the His 215, and the Ala 261 of the polypeptide D2 are suggested to form part of the binding pocket of the Q_a in PSII (Michel & Deisenhofer, 1988; Komiya et al., 1988; Trebst 1986, 1991). These three residues are candidates for the origin of the nitrogen nucleus which is coupled to the Q_A^- radical in PSII.

Although we cannot identify the origin of the nitrogen by means of the ESEEM data alone, useful indications can be obtained by comparison of the ^{14}N nuclear quadrupole resonance (NQR) parameters (K, η) estimated from the present ESEEM data, with NQR parameters that are available in the literature (Hunt & Mackay, 1976; Edmonds, 1977; Ashby et al., 1980). Typical NQR data for ^{14}N concerning the cases under examination are presented in Table 1. A comparison of these values with the ESEEM data shows that the amino nitrogen of the imidazole is most unlikely while the e^2qQ values for the imino nitrogen of the imidazole and the indole nitrogen of the tryptophan approximate the experimental value. In both cases, the values of the asymmetry parameter η seem rather different. For the cases of the peptide nitrogen in small di- and tripeptides, the present ESEEM data seem to be nearly identical to those found by the NQR studies reported in Table 1. There are only a few cases reported of ESEEM data concerning the modulation from an amide nitrogen of the peptide backbone: in fumarate reductase (Cammack et al., 1988) and in the blue copper protein azurin (Coremans et al., 1995), the calculated values for K and η are very similar to those reported here. These comparisons lead us to favor the peptide nitrogen of Ala 261 as the origin of the coupling reported here.

In a recent ESEEM study of the Q_A^- in *R. sphaeroides* where the nonheme iron was substituted by Zn, Bosch et al. (1995) reported the detection of the modulation due to the nucleus of the amino nitrogen of His M219 (equivalent to the His M217 in Ermler et al., 1994). In comparison with our data, this shows the existence of a specific difference in the environment of the semiquinone in low-spin iron-containing PSII compared to Zn-containing reaction centers of *R. sphaeroides*. However, in a report of an ESEEM study of Q_A^- in ironless ^{14}N-PSII which has appeared very recently, some of the modulations were assigned to hyperfine coupling to the amino nitrogen of His (Astashkin et al., 1995) as reported in Zn-containing reaction centers of *R. sphaeroides* (Bosch et al., 1995). Interestingly, in the work of Astashkin et al., a second set of modulations were detected, which were equivalent to those reported here and similarly were assigned to the peptide nitrogen nucleus of Ala 261 of D2 coupled to the Q_A^- (Astaskin et al., 1995). If the assignments of the two sets of modulations in the work of Astashkin et al. are correct, then the experimental data indicate that the two nitrogens (from the His and from the peptide backbone) are not coupled to the *same* Q_A^- radical. Since the authors did not provide any evidence for the presence of combination lines due to multiple ^{14}N couplings [for an analysis of the ESEEM for multiple ^{14}N nuclear coupling see McCracken et al. (1988); see also Mims (1972a) and Lin et al. (1986)], their assignment of the couplings to two ^{14}N coupled to the same radical is questionable. At face value the data of Astashkin et al. should be interpreted as arising from heterogeneous material in which Q_A^- exists in two different environments. These two environments might reflect a population of PSII reaction centers where the iron has been extracted and a population where the iron has been substituted by Zn. Such heterogeneity would not be detected in the c.w. EPR spectrum of the Q_A^- radical (Astashkin et al., 1995; Klimov et al., 1980). This point could probably be clarified by comparison with the ESEEM on the Q_A^- in PSII in which the iron is extracted. Another possible explanation for the differences between the present work and that of Astashkin et al. is that some of the lines in the ESEEM data of Astashkin et al. have origins different from those proposed by the authors. Of note in this respect is that the lines at ~ 1.5 and 4.6 MHz are present in our data but, based on the comparison of ^{14}N to ^{15}N data and the theoretical analysis

(see Results), are attributed to nuclei other than nitrogen and to the double quantum line, respectively.

In the bacterial reaction centers the amide nitrogen of Ala M258 is located at a distance of 3.1 Å in *R viridis* (Michel et al., 1986) or 2.8 Å in *R. sphaeroides* (Ermler et al., 1994) from one of the carbonyl oxygens of the quinone ring to which it is hydrogen bonded. From the discussion given above, taking into account the crystal structure of the bacterial reaction centers, we consider that the peptide backbone nitrogen of the Ala 261 of D2 is the most likely candidate as the origin of the coupling reported here. In the point-dipole approximation, from eq (4c) the coupled nitrogen would be located at a distance ~ 2.7 Å from the closest atom of the semiquinone, i.e., the carbonyl oxygen, assuming that the unpaired spin density is located 100% at the oxygen. For an organic π-orbital system like the semiquinone radical, where the unpaired electron is distributed over the atoms of the quinone ring, the point-dipole model is a rather poor approximation. An improvement could be made by taking the weighted sum of the point-dipole interactions between the nucleus and each atom of the quinone ring. In this case the weights are determined by the fraction of spin density localized on the ring atoms and each atom is treated as a point-dipole interacting with the nucleus of interest (de Beer et al., 1973). An accurate calculation would require a precise knowledge of the spin density distribution in the quinone ring. However, the effective distance scales as the cube root of the spin density reduction factor; therefore, a substantial reduction of the effective spin density on the carbonyl oxygen would have only a modest effect on the calculated O···N distance. In addition, the couplings of the nitrogen with the other, more distant, atoms on the quinone ring would be weaker than to the hydrogen bonded oxygen, and therefore, their contribution would be small. A crude but reasonable estimate of the reduction factor is to take the spin density on the carbonyl oxygen atom to be 0.22 (Feher et al., 1985; MacMillan et al., 1995), making the effective O···N distance ~ 1.6 Å. It is important to note that the point-dipole model can give an underestimation of the real distance (Mims & Peisach, 1978; Kevan, 1990). Nevertheless, the estimate may be useful for comparative purposes in future work.

The hyperfine coupling of the spin of the semiquinone to the nitrogen nucleus on the protein, which we report here (see also Bosch et al. (1995) and Astashkin et al. (1995)] is somewhat surprising given the delocalized π-orbital system of the organic radical and the distances and bonding that are predicted to exist, based on the crystal structure of the bacterial reaction center, between the organic radical and the nitrogen nucleus (i.e., hydrogen bonding from the amide of Ala 261 or the amino group of His 215, or the $\pi-\pi$ overlap between the quinone ring and the indole ring if the N is the nitrogen of the indole ring of Trp 254). The observed isotropic hyperfine coupling is a measure of the unpaired σ-spin density on the coupled nitrogen (Gordy, 1980). The question, however, arises how this spin density migrates onto the nitrogen. There are two basic mechanisms that enter this problem and have been extensively discussed in the literature of organic radicals: spin polarization and/or spin delocalization [for a review see King (1976) and references therein; see also Gordy (1980)]. However, in all the cases the results of calculation depend critically on the assumed structure of the investigated radical. Given the candidates for the origin of the nitrogen coupling discussed above, this information is not available. Thus the data available and the lack of precedence in the literature do not allow for a useful conclusion on the relative importance of the spin transfer mechanisms under consideration. Further studies are required to understand the physical nature of this coupling and to obtain insights on its potential significance to electron transfer. However the observation of nitrogen coupling to the semiquinone radical reported here [see also Bosch et al. (1995) and Astashkin et al. (1995)] provides a precedent that should be relevant to other protein-bound organic radicals.

ACKNOWLEDGMENT

We thank A. J. Hoff (Leiden University, the Netherlands) for communicating results before publication and S. Un for useful discussions. Y.D. expresses his gratitude to V. Petrouleas (NCSR Democritos, Greece) for his support.

REFERENCES

Akabori, K., Kuroiwa, S., & Toyoshima, H. (1992) in *Research in Photosynthesis* (Murata, N., Ed.) Vol. II, p 123, Kluwer Academic Publishers, Dordrecht.
Allen, J. P., Feher, G., Yeats, T. O., Komiya, H., & Rees, D. C. (1988) *Proc. Natl. Acad. Sci. U.S.A. 85*, 8487.
Ashby, C. H., Paron, W. F., & Brown, T. L. (1980) *J. Am. Chem. Soc. 102*, 2290.
Astashkin, A. V., Kawamori, A., Kodera, Y., Kuroiwa, S., & Akabori, K. (1995) *J. Chem. Phys. 102*, 5583.
Berthold, D. A., Babcock, G. T., & Yocum, C. F. (1981) *FEBS Lett. 134*, 231.
Bosch, M. K., Gast, P., Hoff, A. J., Spoalov, A. P., & Tsvetkov, Y. D. (1995) *Chem. Phys. Lett. 239*, 306.
Boussac, A., & Rutherford, A. W. (1988) *Biochemistry 27*, 3476.
Buser, C. A., Diner, B. A., & Brudvig, G. W. (1992) *Biochemistry 31*, 11441.
Calvo, R., Butler, W. F., Isaacson, R. A., Okamura, M. Y., Fredkin, D. R., & Feher, G. (1982) *Biophys. J. 37*, 111a.
Cammack, R., Chapman, A., McCracken, J., Cornelius, J. B., Peisach, J., & Weiner, J. H. (1988) *Biochim. Biophys. Acta 965*, 307.
Coremans, J. W. A., van Gastel, M., Poluektov, O. G., Groenen, E. J. J., den Blaauwen, T., Canters, G. W., Nar, H., Hammann, C., & Messerchmidt, A. (1995) *Chem. Phys. Lett. 235*, 202.
Cornelius, J. B., McCracken, J., Clarkson, R. B., Belford, R. L., & Peisach, J. (1990) *J. Phys. Chem. 94*, 6977.
de Beer, R., De Boer, W., vant Hoff, C. A., & van Ormont, D. (1973) *Acta Crystallogr. Sect. B 29*, 1473.
Debus, R. J., Feher, G., & Okamura, M. Y. (1986) *Biochemistry 25*, 2276.
de Groot, A., Evelo, R., & hoff, A. J. (1986) *J. Magn. Reson. 66*, 331.
Deligiannakis, Y., Diner, B. A., & Petrouleas, V. (1994) *Biochim. Biophys. Acta 1188*, 260.
Dikanov, S. A., & Tsvetkov, Y. D. (1992) *ESEEM Spectroscopy*, CRC Press, Boca Raton.
Dikanov, S. A., Tsvetkov, Y. D., Bowman, M. K., & Astashkin, A. V. (1982) *Chem. Phys. Lett. 90*, 149.
Edmonds, D. T. (1977) *Phys. Rep. C 29*, 233.
Emler, U., Fritzsch, G., Buchanan, S. K., & Michel H. (1994) *Curr. Biol. 2*, 925.
Fauth, J. M., Schweiger, A., Braunschweiler, L., Forrer, J., & Ernst, R. (1986) *J. Magn. Reson. 66*, 64.
Feher, G., Isaacson, R. A., Okamura, M. Y., & Lubitz, W. (1985) *Springer Ser. Chem. Phys. 42*, 174.
Flanagan, H. L., & Singel, D. J. (1987) *J. Chem. Phys. 87*, 5606.
Gerfen, G. J., & Singel, D. J. (1994) *J. Chem. Phys. 100*, 1994.
Gordy, W. (1980) *Theory and Applications of Electron Spin Resonance*, pp 198–304, John Wiley & Sons, Inc., New York.
Hansson, Ö., & Wydrzynski, T. (1990) *Phosynth. Res. 23*, 131.
Hunt, M. J., & Mackay, A. L. (1976) *J. Magn. Reson. 22*, 295.
Kevan, L. (1990) in *Modern Pulsed and Continuous-Wave Electron Spin Resonance* (Kevan, L., & Bowman, M. K., Eds.) Chapter 5, John Wiley & Sons, New York.

King, F. W. (1976) *Chem. Rev. 76*, 157.
Klimov, V. V., Dolan, E., Shaw, E. R., & Ke, B. (1980) *Proc. Natl. Acad. Sci. U.S.A. 77*, 7227.
Komiya, H., Yeates, T. O., Rees, D. C., Allen, J. P., & Feher, G. (1988) *Proc. Natl. Acad. Sci. U.S.A. 85*, 9012.
Koulougliotis, D., Kostopoulos, Th., Petrouleas, V., & Diner, B. A. (1993) *Biochim. Biophys. Acta 1141*, 275.
Koulougliotis, D., Innes, J. B., & Brudvig, G. W. (1994) *Biochemistry 33*, 11814.
Lai, A., Flanagan, H. L., & Singel, D. J. (1988) *J. Chem. Phys. 89*, 7161.
Lin, C. P., Bowman, M. K., & Norris, J. R. (1986) *J. Chem. Phys. 85*, 56.
McCracken, J., Pemper, S., Benkovic, S. J., Villafranca, J. J., Miller, R. J., & Peisach, J. (1988) *J. Am. Chem. Soc. 110*, 1069.
MacMillan, F., Gleiter, G., Renger, H., & Lubitz, W. (1989) in *Current Research in Photosynthesis* (Baltcheffsky, M., Ed.) Vol. 1, p 531, Kluwer, Dordrecht.
MacMillan, F., Lendzian, F., Renger, H., & Lubitz, W. (1995) *Biochemistry 34*, 8144.
Michel, H., Epp, O., & Deisenhofer, J. (1986) *EMBO J. 5*, 2445.
Michel, H., & Deisenhofer, J. (1988) *Biochemistry 27*, 1.
Mims, W. B. (1972a) *Phys. Rev. B5*, 2409.
Mims, W. B. (1972b) *Phys. Rev. B6*, 3543.
Mims, W. B. (1984) *J. Magn. Reson. 59*, 291.
Mims, W. B., & Peisach, J. (1978) *J. Chem. Phys. 69*, 4921.
Mims, W. B., & Peisach, J. (1981) in *Biological Magnetic Resonance*, Vol. 3, Chapter 5, Plenum Press, New York.
Nugent, J. H. A., Diner, B. A., & Evans, M. C. W. (1981) *FEBS Lett. 124*, 241.
Petrouleas, V., & Diner, B. A. (1987) *Biochim. Biophys. Acta 893*, 126.
Plato, M., Michel-Beyrle, M. E., Bixon, M., & Jortner, J. (1989) *FEBS Lett. 1*, 70.
Reijerse, E. J., & Dikanov, S. A. (1991) *J. Chem. Phys. 95*, 836.
Reijerse, E. J., & Keijers, C. P. (1987) *J. Magn. Reson. 71*, 83.
Romanelli, M., Goldfarb, D., & Kevan, L. (1988) *Magn. Reson. Rev. 13*, 179.
Rutherford, A. W., & Zimmermann, J. L. (1984) *Biochim. Biophys. Acta 767* 168.
Sanakis, Y., Petrouleas, V., & Diner, B. A. (1994) *Biochemistry 33*, 9922.
Trebst, A. (1986) *Z. Naturforsch. 41c*, 240.
Trebst, A. (1991) *Z. Naturforsch. 46c*, 557.
Vermaas, W. F. J., & Rutherford, A. W. (1984) *FEBS Lett. 175*, 243.
Zimmermann, J. L.; Boussac, A., & Rutherford, A. W. (1993) *Biochemistry 32*, 4831.

BI951601J